Journal of Quantitative Spectroscopy & Radiative Transfer 270 (2021) 107697

Contents lists available at ScienceDirect

Journal of Quantitative Spectroscopy & Radiative Transfer

journal homepage: www.elsevier.com/locate/jqsrt

Automatic methods for gas absorption calculation based on correlated k-distribution

Mingwei Zhu[a], Shuanggen Jin[a,b,*], Ju Tao[c], Xinyue Wu[d]

[a] School of Remote Sensing and Geomatics Engineering, Nanjing University of Information Science and Technology, Nanjing 210044, China
[b] Shanghai Astronomical Observatory, Chinese Academy of Sciences, Shanghai 200030, China
[c] Ningbo Meteorological Safety and Technology Center, Ningbo 315010, China
[d] Zhenjiang Meteorological Bureau, Zhenjiang 212003, China

ARTICLE INFO

Article history:
Received 4 January 2021
Revised 17 March 2021
Accepted 7 April 2021
Available online 29 April 2021

Keywords:
Correlated k-distribution model
Finding point method
Gas absorption calculation
Optimization method

ABSTRACT

Several schemes have been proposed for handling gaseous overlapping bands in the context of the correlated k-distribution model (CKD), but they all require manual operation and the accuracy is limited. In this paper, we proposed two automatic methods for gas absorption calculation based on correlated k-distribution, namely finding point method (FPM) and re-optimized method (ROM), to improve the accuracy and the speed of gaseous absorption calculation. Compared with the line-by-line (LBL) results under standard profiles, the resulting accuracy of FPM is 0.09 $Kday^{-1}$ in troposphere, -0.3 $Kday^{-1}$ in stratosphere, -0.18 W/m^2 for upward flux and -0.44 W/m^2 for downward flux; the accuracy of ROM is 0.1 $Kday^{-1}$ in troposphere, 0.3 $Kday^{-1}$ in stratosphere, -0.35 W/m^2 for upward flux and -0.18 W/m^2 for downward flux. The accuracy of the two methods is higher than rapid radiative transfer model for general circulation models (RRTMG). Under realistic profiles, the accuracy of FPM and ROM is slightly lower than that their accuracy under standard profiles but still higher than RRTMG.

1. Introduction

Radiative absorption of the atmosphere is a crucial component of various atmospheric models, especially for long-term climate simulations. The radiative calculation in climate studies requires high accuracy and fast speed. Line-by-line (LBL) radiative transfer method [1,2,3] is the most precise way to simulate the atmospheric radiative transfer process, but its calculation amount is too large for practical problems [4,5]. Over the past decades, correlated k-distribution model (CKD) has been widely adopted in thermal infrared radiative transfer calculations for its particularly simple and practical property [6–11]. In CKD, the gaseous absorption within a spectral interval is assumed to be unrelated to the variation of the absorption coefficient for wavenumber, and gaseous absorption is contingent only on the distribution of k within the spectral interval [8,12,13,14]. Then, the absorption coefficients can be sorted in order of increasing intensity, and the gaseous transmission can be integrated over a smooth and monotonically increasing absorption coefficient space instead of over a tortuously variable frequency space. Therefore, the CKD method requires fewer points to calculate the spectral transmissivity than the LBL calculation. In other words, CKD method is much more efficient than the LBL, and is relatively accurate in solving the gaseous absorption and multiple scattering in inhomogeneous atmosphere involving aerosols and clouds [10]. Atmospheric and Environmental Research Inc. (AER) developed the Rapid Radiative Transfer Model (RRTM) [15]. This model is highly accurate due to the efficient schemes for gas absorption calculations optimized by the LBL model for the high-resolution transmission (HITRAN) database. The European Center of Middle-Range Weather Forecast (ECMWF) developed abroad band radiation scheme [16] for their general circulation model (GCM), which has been replaced by a rapid version of RRTM (RRTMG for General Circulation Models (RRTMG)) since 2000 [17].

An essential problem of CKD method is how to deal with the numerous overlapping absorption bands in the thermal infrared region. Since Wang and Ryan [18] investigated the overlapping effects of atmospheric gases absorption, several studies tried to solve the overlapping problem in the context of CKD. The very first method is based on the multiplication property of transmission. In the approach, the total transmission of a gas mixture is equal to the product of the transmissions by the individual gases. However, this property can only be applied to monochromatic transmission or to spectrally averaged transmission of a small spectral interval. For a wide absorption band, the multiplication property is

* Corresponding author.
E-mail addresses: sgjin@nuist.edu.cn, sgjin@shao.ac.cn (S. Jin).

https://doi.org/10.1016/j.jqsrt.2021.107697
0022-4073/

Nomenclature

a_i	Position point for ith Gaussian quadrature point
α	adjusted factor
$c_{x_i,\ P_j^r,i}$	The ith fitting coefficient for temperature in x_i integration point and jth reference pressure
$f(k)$	probability density
f_{obj}	objective function
F_{err}	error function of flux
$F_{TOA.LBL}^{\uparrow}$	LBL calculated value of upward flux at the top of the atmosphere
$F_{TOA}^{\uparrow}$	CKD calculated value of upward flux at the top of the atmosphere
$F_{sfc.LBL}^{\downarrow}$	LBL calculated value of downward flux at surface
$F_{sfc}^{\downarrow}$	CKD calculated value of downward flux at surface
g	cumulative probability function
Δg_i	Weight point for ith CKD integration point
$\Delta G_{i_1,i_2}$	weight of CKD integration point $p(i_1,i_2)$
h	CKD calculated value of heating rate
h_{LBL}	LBL calculated value of heating rate
H_{err}	error function of heating rate
k	absorption coefficient
k^r	absorption coefficient in reference pressure
k_{max}	maximum absorption coefficient in reference level
n	total number of CKD integration points
$p(i_1,i_2)$	Combination point consisted of x_{i_1} of gas 1 and x_{i_2} of gas 2
P	Atmospheric pressure
P_j^r	jth reference pressure
r	Ratio of heating rate error function
T	Atmospheric temperature
Tr	transmission
v	wavenumber
Δv	spectral interval
w_i	weight for ith Gaussian quadrature point
x_i	Position point for ith CKD integration point

only valid when spectral features of all the overlapping gases are perfectly uncorrelated. However, for most practical situations, this scheme is not applicable due to the non-random-induced correlation [10]. Li and Barker [9] took partly correlation into account and further modified the partly correlation scheme algorithm as an alternate mapping method. In this method, cumulative probability space is divided into several intervals and then one primary gas is assumed to dominate the absorption in each interval, while the same sorting rule is applied to the other gases in this interval. However, it requires manual effort in building the algorithm compared to the band-mean models. For example, it needs to try to choose different interval divisions and gases in each interval [5,9]. Therefore, the accuracy is limited by the manual operation. To circumvent the overlapping problem, some studies focused on the modified amount weighted scheme. The main idea of this scheme is combining these coefficients by weighting absorber amounts into the "single gas". Therefore, the key is to find a comprehensible and efficient way to generate combined spectral parameters for the "single gas" that are related to those of the individual gases. While this method has achieved high accuracy, its handling of weighting factors for each gas becomes inefficient for bands with more than two absorbers [9,10].

Is this study, we aimed to find a non-manual scheme to improve the accuracy and the speed of CKD method. Therefore, we proposed two automatic methods inspired by decreasing method (DM) [19,20], called finding point method (FPM) and re-optimized method (ROM) for gas absorption calculation in an atmospheric general circulation model. In Section 2, we introduced the CKD theory, DM, FPM and ROM. In Section 3, we used the wavenumber ranges, implemented gas species and the number of k-distribution points in RRTMG in our calculation, and compared the results based on FPM and ROM with those based on RRTMG. Finally conclusions are given in Section 4.

2. Correlated k-distribution model theory

In CKD method, the transmission of a single gas can be expressed as an integration over the cumulative probability and evaluated by a finite sum of exponential terms [10]:

$$\begin{aligned} Tr &= \tfrac{1}{\Delta v}\int_{\Delta v} e^{-k(v)u}dv \\ &= \int_0^\infty f(k)e^{-ku}dk \\ &= \int_0^1 e^{-k(g)u}dg \\ &= \sum_{i=1}^{n} e^{-k(x_i)u}\Delta g_i \end{aligned} \tag{1}$$

Where Tr is the transmission; v is wavenumber and Δv is the spectral interval; u is the absorber amount; k is the absorption coefficient; $f(k)$ is the probability density; g is the cumulative probability function; x_i and Δg_i are integration point and weight for ith point; n is the total number of integration points. For x_i and Δg_i, the constraints are as follows [10]:

$$\sum_{i=1}^{n}\Delta g_i = 1. \tag{2}$$

The inequality constraints are as follows:

$$\begin{cases} \Delta g_i > 0 \\ 0 < x_i < 1 \end{cases} (i = 1, \cdots,\ n). \tag{3}$$

In spectral bands, the absorption coefficients change drastically in the cumulative space close to 1. Therefore, the quadrature points x_i and weights Δg_i are set as follow [20]:

$$\begin{cases} \Delta g_i = 2\Delta w_i a_i \\ x_i = {a_i}^2, \end{cases} \tag{4}$$

where a_i and w_i are Gaussian quadrature point and weight for ith point. In the realistic inhomogeneous atmosphere, $k(x_i)$ is influenced by variable pressure P and temperature T of inhomogeneous atmosphere. Therefore, $k(x_i)$ becomes $k(x_i,P,T)$. CKD method assumes that the ordering of the strengths of absorption lines is the same as those of different temperature T and pressure P levels. Then, $k(x_i,P,T)$ is parameterized as a function of temperature polynomial for multiple reference pressures. In the jth reference pressure, the absorption coefficient can be obtained by [5,9]:

$$k^r\left(x_i, P_j^r, T\right) = \sum_{t=1}^{5} c_{x_i,P_j^r,t} * (T-250)^{t-1}, \tag{5}$$

where P_j^r is the jth reference pressure, and $c_{x_i,\ P_j^r,i}$ is the fitting coefficient for temperature in each integration point and reference pressure. A total of 21 reference pressure levels are distributed between 1000 and 0.1 mb, which are 1000, 630.957, 398.107, 251.189, 158.489, 100, 63.096, 39.811, 25.119, 15.849, 10, 6.31, 3.981, 2.512, 1.585, 1, 0.631, 0.398, 0.251, 0.158, 0.1 mb. Equations (5) are valid for temperatures between 160 and 340 K, which includes most atmospheric conditions [9]. Then the absorption coefficient $k(x_i,P,T)$ at any arbitrary pressure P can be approximated by the linear interpolation between two neighboring P_j^r and P_{j+1}^r $(P_j^r < P < P_{j+1}^r)$ through the equation:

$$k(x_i,P,T) = \frac{P_j^r - P}{P_j^r - P_{j+1}^r}\cdot\left[k^r\left(x_i,P_{j+1}^r,T\right) - k^r\left(x_i,P_j^r,T\right)\right] + k^r\left(x_i,P_j^r,T\right). \tag{6}$$

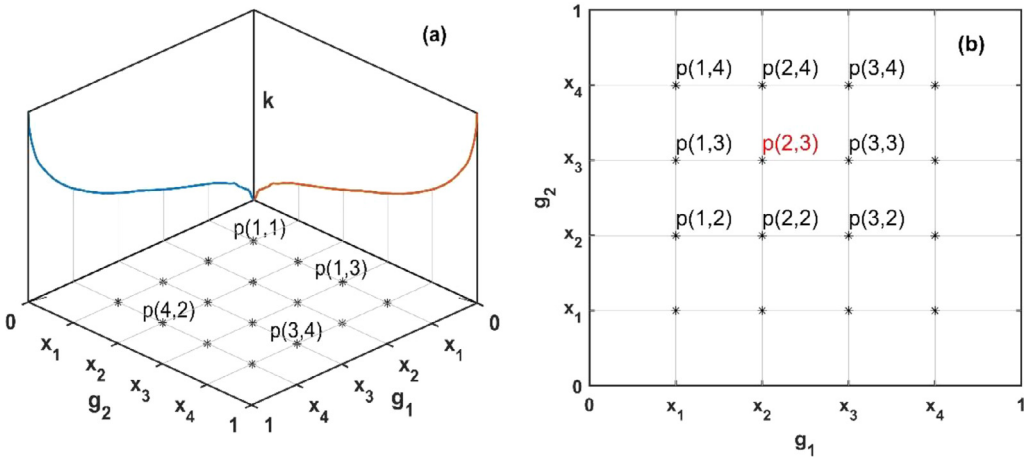

Fig. 1. Treatment of overlapping band absorption for two gases in the k-distribution method.

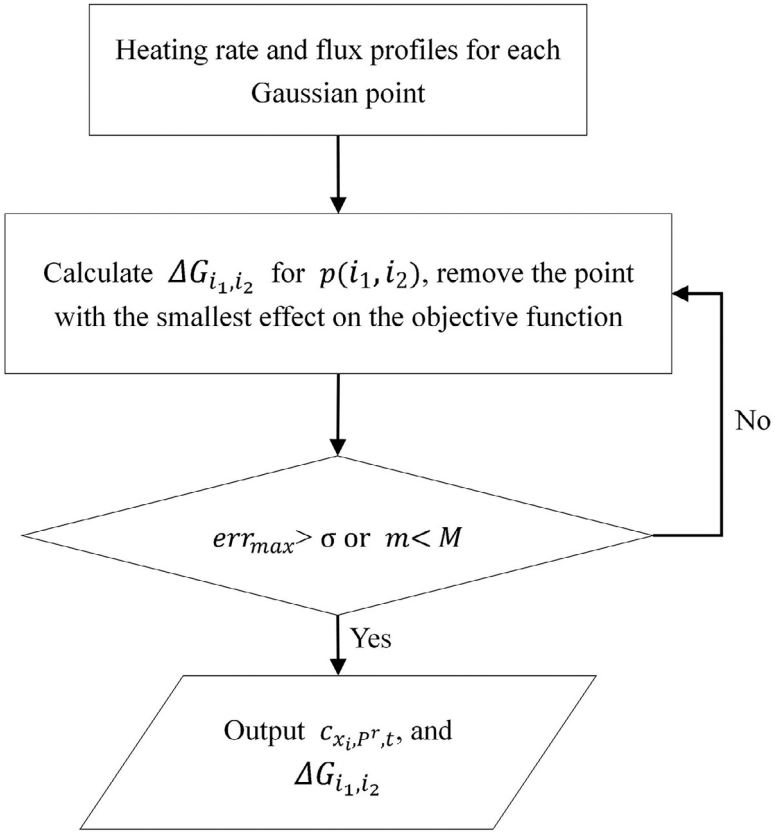

Fig. 2. Flow chart of DM.

Table 1
Points' serial numbers for different number of points in 1380-1490cm^{-1} band.

Number of integration points	Serial number of p
1	8
2	8,19
3	8,17,19
4	6,11,18,20
5	6,11,15,18,20
6	5,9,13,17,18,19
7	5,9,13,17,18,19,20

For the pressure lower than P_1^r or larger than P_{21}^r, we use linear extrapolation to calculate the coefficient.

2.1. Decreasing Method

Decreasing method is an improved method of the traditional CKD theory [20]. It adopts a nonlinear optimization method to decrease the number of quadrature points, and get more accurate quadrature points and weights and optimize the overlapping problem simultaneously. We can regard the heating rate and radiative flux result calculated by LBL and those results calculated by CKD in each quadrature point as vectors in a high-dimensional space. In other words, we need to linearly combine those vectors of each

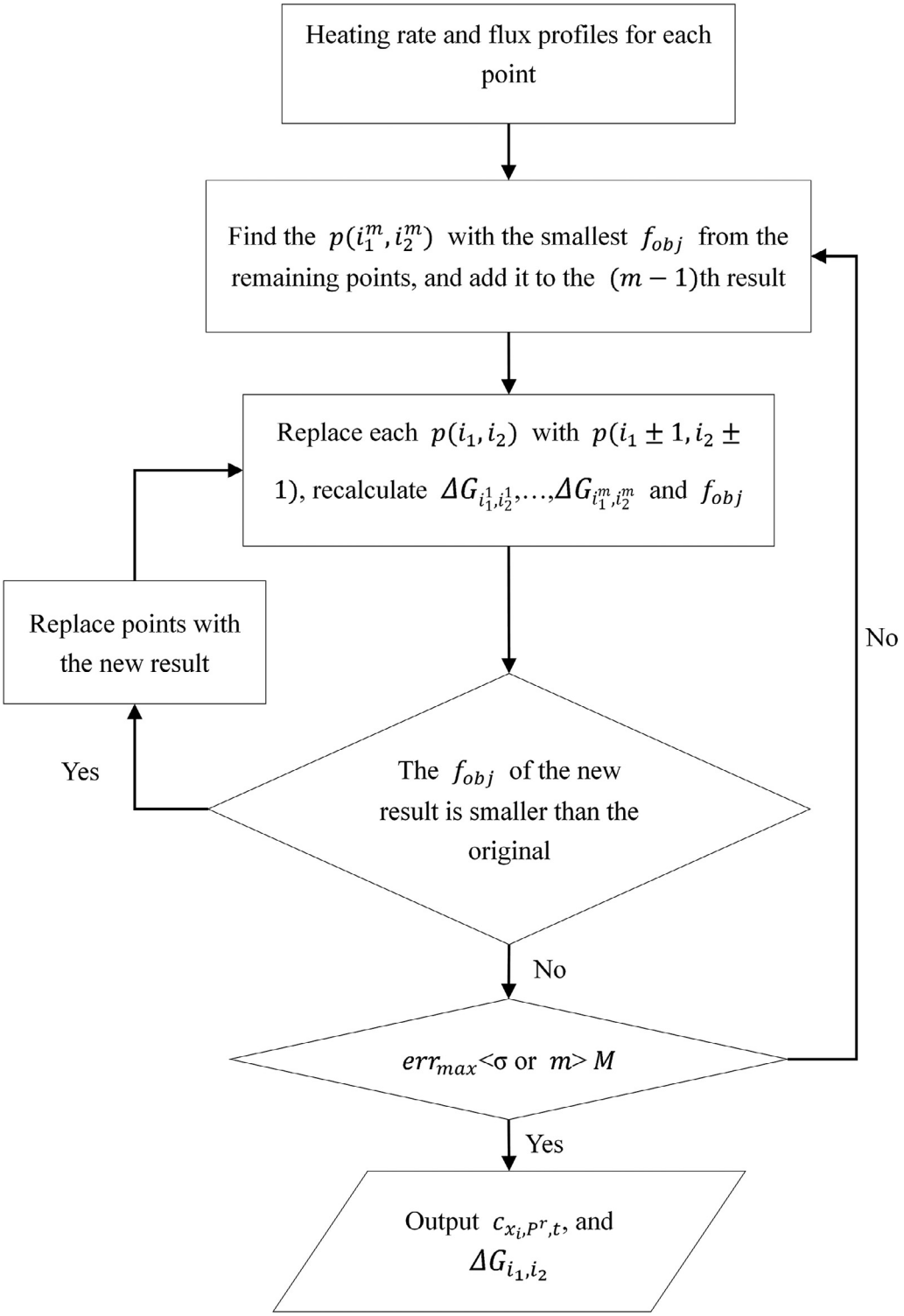

Fig. 3. Flow chart of FPM.

CKD points into the vector of LBL. For constrained linear addition, there is usually only one optimal solution for a given target vector and several optimization vectors. In this study, the sequential quadratic programming (SQP) [21] is used as optimization method, the number of Gaussian quadrature points is 20, and the number of SQP iteration is 100. In the above optimization problems, the objective function is

$$f_{obj}(\Delta g_1, \Delta g_2, \ldots, \Delta g_M) = \sqrt{\sum_{iatm=1}^{6} \left(F_{err}(iatm)^2 + rH_{err}(iatm)^2\right)/6}, \quad (7)$$

where Δg_1,Δg_2,..., Δg_M are the weights of M integration points; $iatm$ is $iatm$th atmospheric profile; r is the ratio that set as 0.01 [19]; F_{err} and H_{err} are the error functions of flux and heating rate, respectively. The definition of F_{err} and H_{err} are as follows

$$F_{err}(iatm) = \sqrt{\frac{\sum_{l=1}^{NL}\left(F_{TOA}^{\uparrow}(iatm, \Delta g_1, \Delta g_2, \ldots, \Delta g_M) - F_{TOA.LBL}^{\uparrow}(iatm)\right)^2}{\sum_{l=1}^{NL} F_{LBL}^{\uparrow}(iatm)^2}}$$

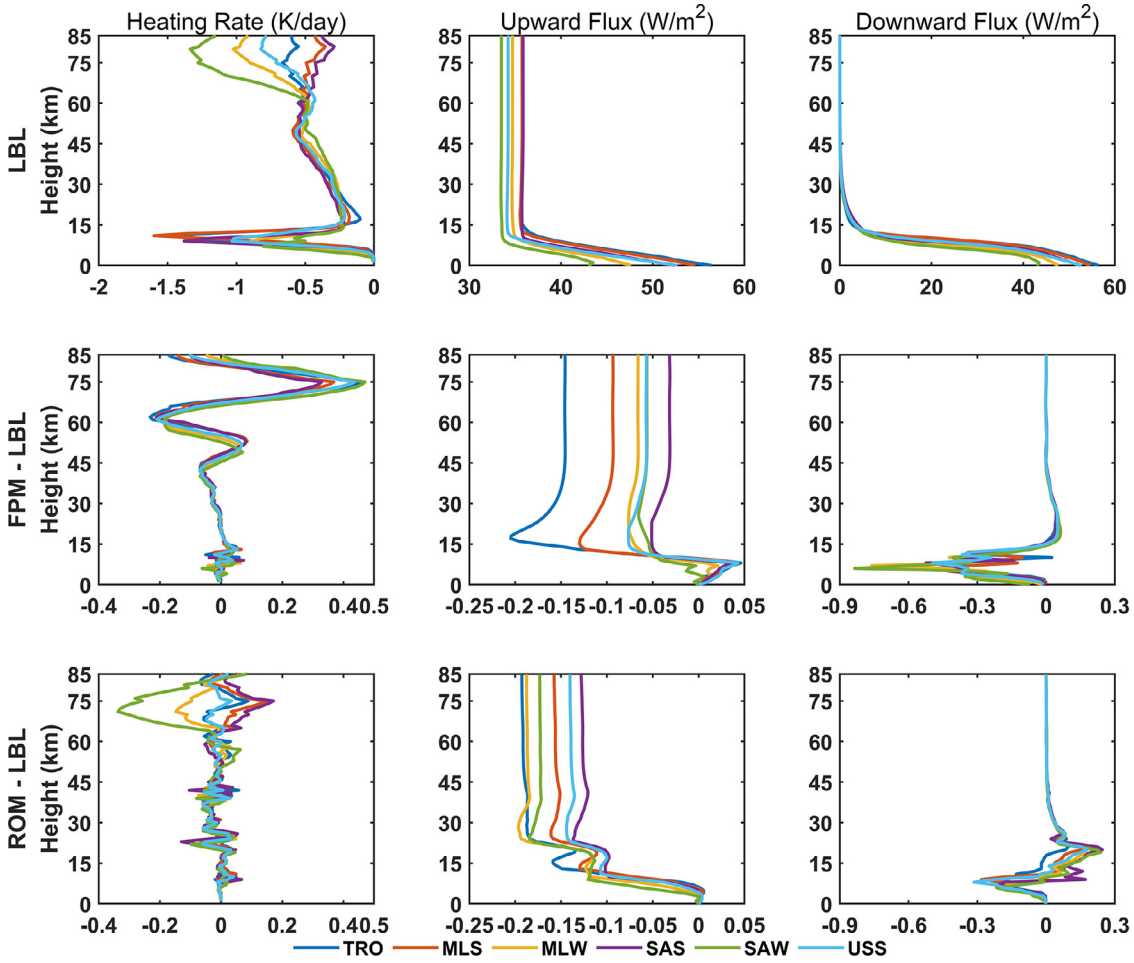

Fig. 4. Heating rates and fluxes calculated by LBL (top panels), and the errors of FPM (middle panels) and ROM (bottom panels) in 10 - 350 cm^{-1} band under six standard profiles.

Table 2
Objective function of optimal solution and the error of DM and FPM for different number of points in 1380-1490cm^{-1} band.

Number of points	Optimal solution	DM - optimal solution	FPM - optimal solution
1	$6.7654*10^{-2}$	$22.2172*10^{-2}$	0
2	$1.9832*10^{-2}$	$3.3673*10^{-2}$	0
3	$5.9994*10^{-3}$	$47.0662*10^{-3}$	$2.8328*10^{-3}$
4	$1.8945*10^{-3}$	$3.9551*10^{-3}$	$2.3912*10^{-3}$
5	$6.9314*10^{-4}$	$51.1492*10^{-4}$	$0.7265*10^{-4}$
6	$4.9835*10^{-4}$	$12.3163*10^{-4}$	0
7	$4.1524*10^{-4}$	$0.6526*10^{-4}$	0

$$+\sqrt{\frac{\sum_{l=1}^{NL}\left(F_{sfc}^{\downarrow}(iatm,\Delta g_1,\Delta g_2,\ldots,\Delta g_M)-F_{sfc.LBL}^{\downarrow}(iatm)\right)^2}{\sum_{l=1}^{NL}F_{LBL}^{\downarrow}(iatm,l)^2}}, \tag{8}$$

$$H_{err}(iatm)=\sqrt{\frac{\sum_{l=1}^{NL}\left(h(iatm,l,\Delta g_1,\Delta g_2,\ldots,\Delta g_M)-h_{LBL}(iatm,l)\right)^2}{\sum_{l=1}^{NL}h_{LBL}(iatm,l)^2}}, \tag{9}$$

where $F_{TOA.LBL}^{\uparrow}$, $F_{sfc.LBL}^{\downarrow}$ and h_{LBL} are the LBL calculated value of upward flux at the top of the atmosphere (TOA), downward flux at surface and heating rate, respectively; $F_{TOA}^{\uparrow}$, $F_{sfc}^{\downarrow}$ and h are the CKD calculated value of upward flux at the TOA, downward flux at surface and heating rate, respectively; l is the lth level for atmospheric profiles. Six standard atmospheric profiles are considered in study, namely tropical (TRO), mid-latitude summer (MLS), mid-latitude winter (MLW), sub-arctic summer (SAS), sub-arctic winter (SAW) and United States standard (USS) [22]. For the spectral bands with multiple gas absorptions need to be considered, DM assumes that the cumulative probability functions of gases are perfectly uncorrelated, and the transmission equation becomes:

$$Tr=\sum_{i_1=1}^{n}\sum_{i_2=1}^{n}\cdots\sum_{i_{nmol}=1}^{n}\Delta g_{i_1}\Delta g_{i_2}\cdots\Delta g_{i_{nmol}}\exp\left[-\left(\sum_{j=1}^{nmol}k_j(x_{i_j})u_j\right)\right], \tag{10}$$

where x_{i_j} and Δg_{i_j} are an ith quadrature point and its weight of numerical integration for the jth gas, and $nmol$ is the number of absorption gases in a spectral band. The number of quadrature

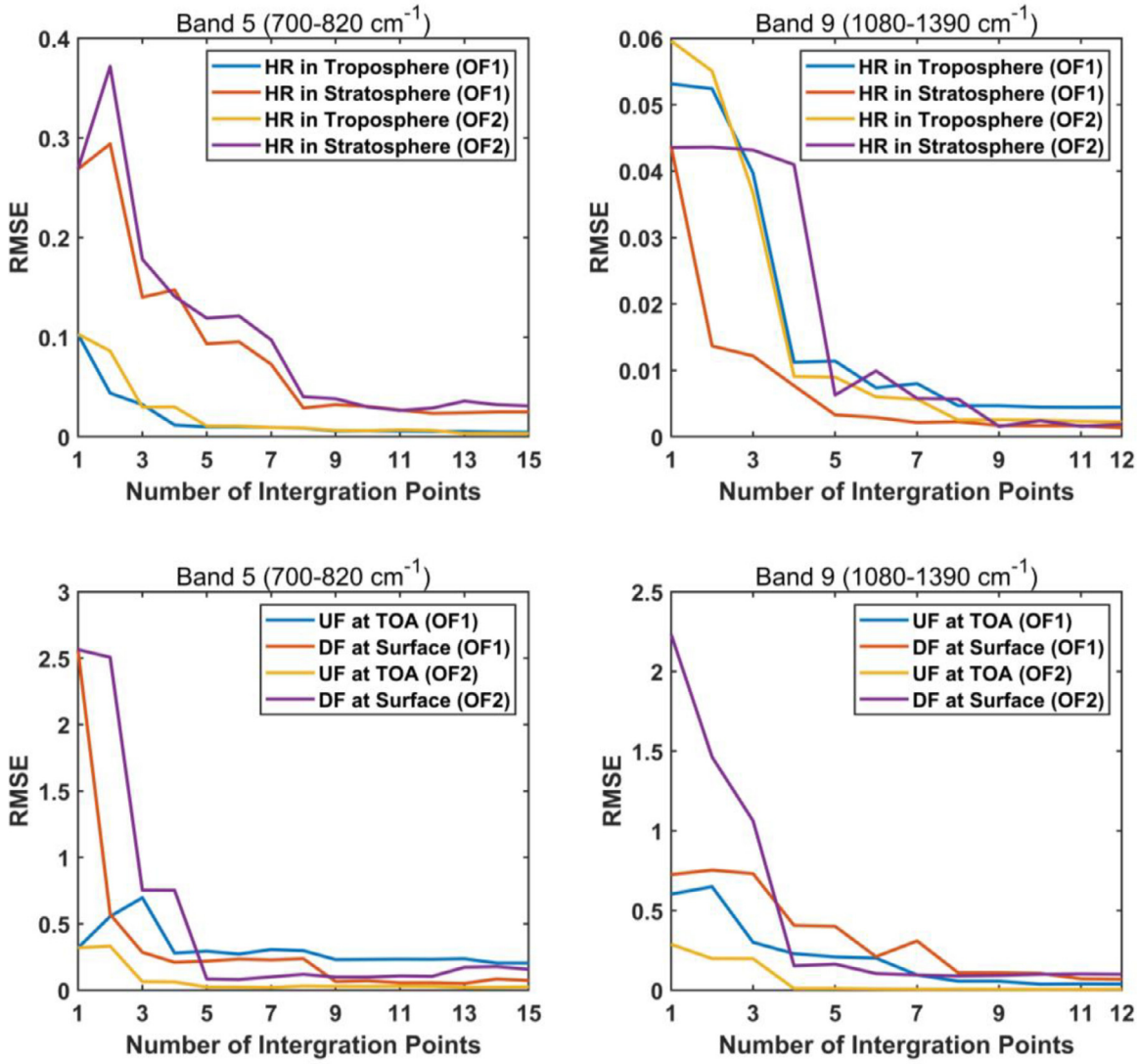

Fig. 5. RMSE of the two objective functions versus the number of integration points in the band 5 (700-820 cm^{-1}) and band 9 (1180-1390 cm^{-1}). * HR: Heating Rate. UF: Upward Flux. DF: Downward Flux.

Table 3
Errors of ROM, FPM and RRTMG under six standard profiles.

	ROM	FPM	RRTMG
RMSE of HR in Stratosphere	0.0806	0.0872	0.2161
ME of HR in Stratosphere	-0.2936	-0.2995	0.9372
RMSE of HR in Troposphere	0.0214	0.0315	0.0551
ME of HR in Troposphere	0.0923	-0.0834	0.1460
RMSE of UF at TOA	0.2896	0.1219	0.5496
ME of UF at TOA	-0.3496	-0.1766	0.7808
RMSE of DF at Surface	0.0834	0.2448	1.0763
ME of DF at Surface	-0.1793	-0.4395	-1.2147

* ME: maximum error. HR: heating rate. UF: upward flux. DF: downward flux. The unit of heating rate is $Kday^{-1}$, and the unit of flux is Wm^{-2}

Table 4
Errors of ROM, FPM and RRTMG in doubling CO2 concentration under six standard profiles.

	ROM	FPM	RRTMG
RMSE of HR in Stratosphere	0.0753	0.1214	0.1876
ME of HR in Stratosphere	-0.2790	0.4494	0.6761
RMSE of HR in Troposphere	0.0226	0.0315	0.0558
ME of HR in Troposphere	0.0972	0.0828	0.1476
RMSE of UF at TOA	0.2481	0.1142	0.4282
ME of UF at TOA	-0.3002	-0.1420	0.6102
RMSE of DF at Surface	0.0794	0.1451	0.9000
ME of DF at Surface	-0.1778	-0.2150	-1.0809

* ME: maximum error. HR: heating rate. UF: upward flux. DF: downward flux. The unit of heating rate is $Kday^{-1}$, and the unit of flux is Wm^{-2}

points is $m = n^{nmol}$. We assume there are two gases in this example, and Eq. 10 becomes:

$$\begin{aligned} Tr &= \sum_{i_1=1}^{n}\sum_{i_2=1}^{n} \Delta g_{i_1}\Delta g_{i_2} \exp\left[-\left(k_1(x_{i_1})u_1 + k_1(x_{i_2})u_2\right)\right] \\ &= \sum_{i_1=1}^{n}\sum_{i_2=1}^{n} \Delta G_{i_1,i_2} \exp\left[-\left(k_1(x_{i_1})u_1 + k_1(x_{i_2})u_2\right)\right] \end{aligned} \tag{11}$$

We can get combinations of x_{i_1} and x_{i_2} which showed in Fig. 1. Each x_{i_1} and x_{i_2} can be combined into a point $p(i_1,i_2)$, and the weight of $p(i_1,i_2)$ is $\Delta G_{i_1,i_2} = \Delta g_{i_1}\Delta g_{i_2}$.

Fig. 2 shows the flow chart of DM. When the optimization process has converged, the point with the smallest effect on the objective function is removed from the solution of the mth order, that is, remove the point from the grid of Fig. 1. then this removed

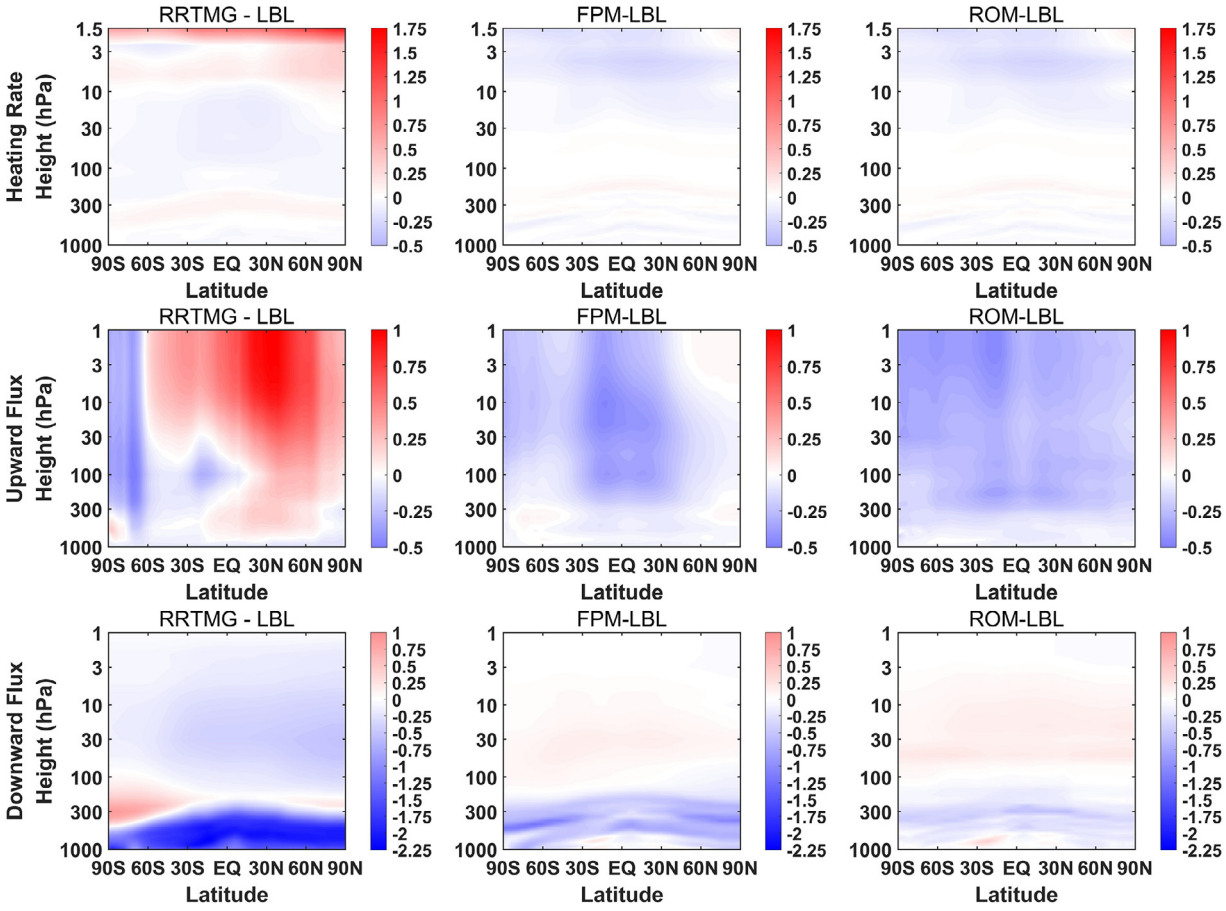

Fig. 6. Error contours for latitude-pressures calculated by RRTMG, FPM and ROM. The units of heating rate and flux are $Kday^{-1}$ and Wm^{-2}, respectively.

condition is used as the initial condition for the $(m-1)$th order. The operation is repeated for all orders until the maximum error err_{max} larger than prescribed value σ, or the number of points m is smaller than objective number M.

2.2. Finding point method

As the DM described, the result with less points must be included in the result with more points. However, as the Gaussian quadrature points are prescribed, the result with less points is not included in the result with more points for most situations. To illustrate this problem, we used the exhaustive method to get the global optimal solution in 1380-1490 cm^{-1} band, and only one absorption gas is considered in this band. Therefore, $p(i_1,i_2)$ defined in Fig. 1 becomes $p(i_1)$. The results are showed in Table 1. The points in optimal solution with three points is point $p(8)$, $p(17)$ and $p(19)$, while the optimal solution with four points is $p(6)$, $p(11)$, $p(18)$ and $p(20)$. Therefore, the accuracy of DM is low when the number of points is small.

Based on the problem that the points in combinations with different number of points are different, we proposed the finding points method (FPM) described in Fig. 3. We assume there are two gases in this example, and define $p(i_1^m, i_2^m)$ as the mth point in the solution. Fisrt, we prescribed the Gaussian quadrature points as 20, and find the optimal solution with one point $p(i_1^1, i_2^1)$. Second, we find $p(i_1^2, i_2^2)$ in the remaining points, so that its combination with $p(i_1^1, i_2^1)$ can be the optimal combination. The weights of $[p(i_1^1, i_2^1),\ p(i_1^2, i_2^2)]$ are g_1 and g_2, respectively. Next, we use the adjacent points of each point in turn, namely $p(i_1^1 \pm 1, i_{21}^1 \pm 1)$ and $p(i_1^2 \pm 1, i_2^2 \pm 1)$ to replace the original points, and recalculate the weights by optimization method. For example, we assume the first point is $p(2, 3)$, then $P(2 \pm 1, 3 \pm 1)$ (i.e. $p(1, 4)$, $p(1, 3)$, $p(1, 2)$, $p(2, 2)$, $p(3, 2)$, $p(3, 3)$, $p(3, 4)$, and $p(2, 4)$ showed in Fig. 1b) are the adjacent points of $p(2, 3)$. We replace the original point combination with a smaller error combination until the error reaches a minimum. Finally, we go to the first step to add point $p(i_1^m, i_2^m)$ for the mth order and repeat the process until the maximum error err_{max} is less than prescribed value σ, or the number of points m is larger than the objective number M.

Table 2 shows the global optimal solution in the objective functions in 1380-1490cm^{-1} band and the errors of DM, FPM. The global optimal solution is obtained by exhaustive method. For both DM and FPM, the errors decrease when the number of point increases. In all cases, the objective function errors of FPM are less than DM. For one, two, six and seven quadrature point cases, FPM can get the optimal solution. Besides, since FPM calculates fewer quadrature points in optimization, compared to DM that needs to iterate from n^{nmol} quadrature points, the iteration time of FPM is greatly shortened

2.3. Re-optimized method

After the operation of FPM, we get a satisfying result with a small number of points. However, the accuracy of results is limited by the number of prescribed Gaussian quadrature points. Thus, we use an adjusted factor to minimize the objective function, and the optimization method is used again when calculating the adjust factor. This method is called re-optimized method (ROM). The

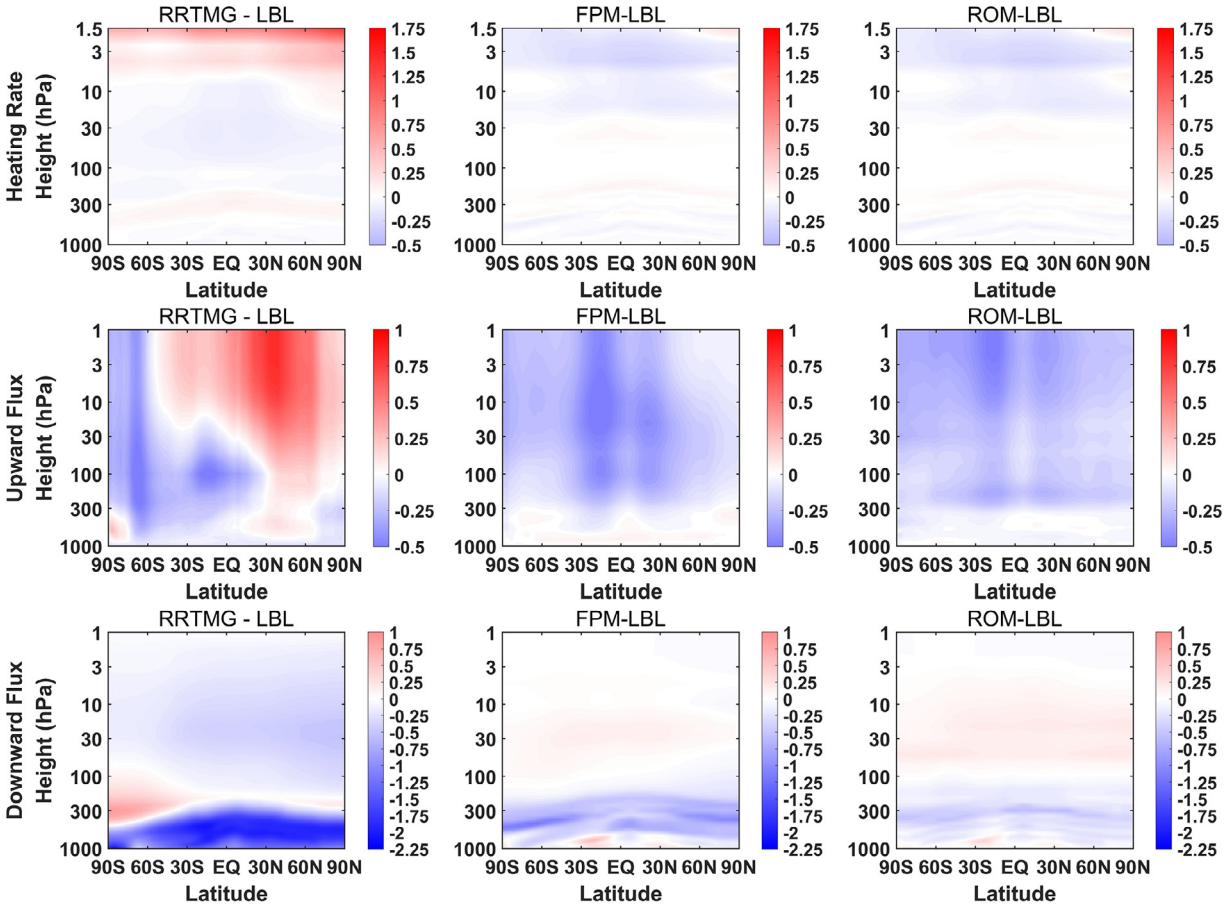

Fig. 7. Error contours for latitude-pressures calculated by RRTMG, FPM and ROM in double CO2 concentration condition. The units of heating rate and flux are $Kday^{-1}$ and Wm^{-2}, respectively.

constraints of optimization method are:

$$\begin{cases} \alpha * k^r(x_i, P^r, T) > 0 \\ \alpha * k^r(x_i, P^r, T) - k_{max}(P^r, T) \le 0 \end{cases} \tag{12}$$

where α is the adjusted factor; k_{max} is the maximum absorption coefficient in each reference level, and it can be obtained from LBL and expressed as a function of temperature polynomial: $k_{max}(P^r, T) = \sum_{t=1}^{5} c_{P^r,t}^{max} * (T - 250)^{t-1}$, where $c_{P^r,t}^{max}$ is fitting coefficient for temperature in each reference pressure. The first inequality constraint indicates that the absorption coefficient at each integration point calculated by ROM must always be greater than 0, i.e. $\alpha > 0$. The second inequality constraint means that the absorption coefficient at each quadrature point calculated by ROM must be always less than the maximum absorption coefficient k_{max}. k_{max} is obtained from LBL and approximated with the polynomial of temperature. The form of the polynomial is the same as k^r, which is showed in Eq.5. Since k^r and k_{max} in Eq. (12) are all fourth-order polynomials of temperature, here we use the first derivative of the absorption coefficient polynomial to find the largest value as the maximum lies at the boundary of the temperature range or at the stable point with derivative zero, and make the largest value lower than 0. Normally, the value of α fluctuates around 1.

To illustrate the accuracy of FPM and ROM, we calculated the heating rates and radiative fluxes by LBL (top panels), the errors of FPM (middle panels) and the errors of ROM (bottom panels) in 10 - 350 cm^{-1} band under standard profiles. As shown in Fig. 4, the heating rate errors of ROM are less than FPM at the height over 40 km. At the remaining heights, heating rate errors of ROM are comparable with FPM. For the upward flux, the errors of ROM are less than FPM at the height below 20 km. FPM has a maximum error over -0.2 W/m^2 in 17 km height under TRO profile, while the maximum error of ROM is about 0.16 W/m^2 in 15 km under TRO profile. In the higher atmosphere, ROM is less accurate. At TOA, the flux errors of ROM are larger than -0.1 W/m^2, while the error of FPM fluctuate between -0.03 W/m^2 and -0.15 W/m^2. For the downward flux, ROM is more accurate than FPM below 15 km. The maximum error of FPM is over -0.8 W/m^2 under SAW profile. In contrast, the errors of ROM do not reach 0.3 W/m^2 at all heights, which is less than a half that of FPM. In the height between 15 km and 30 km, ROM is less accurate. ROM is not better than FPM in all results. This is because in the secondary optimization process of ROM, in order to minimize the objective function, SQP reduces the large value in the error, but sometimes also makes the small value larger. The error distribution ends up becoming more uniform. For some spectral bands, such as 1390 – 1480 cm^{-1}, the accuracy of ROM is higher than FPM in all results.

3. Results and Analysis

3.1. Objective function

We defined two objective functions in our study: objective function 1 (OF1)

$$f_{obj}^1(\Delta g_1, \Delta g_2, \ldots, \Delta g_M) = \sqrt{\sum_{iatm=1}^{6} \left(F_{err}^1(iatm)^2 + rH_{err}^1(iatm)^2\right)/6}, \tag{13}$$

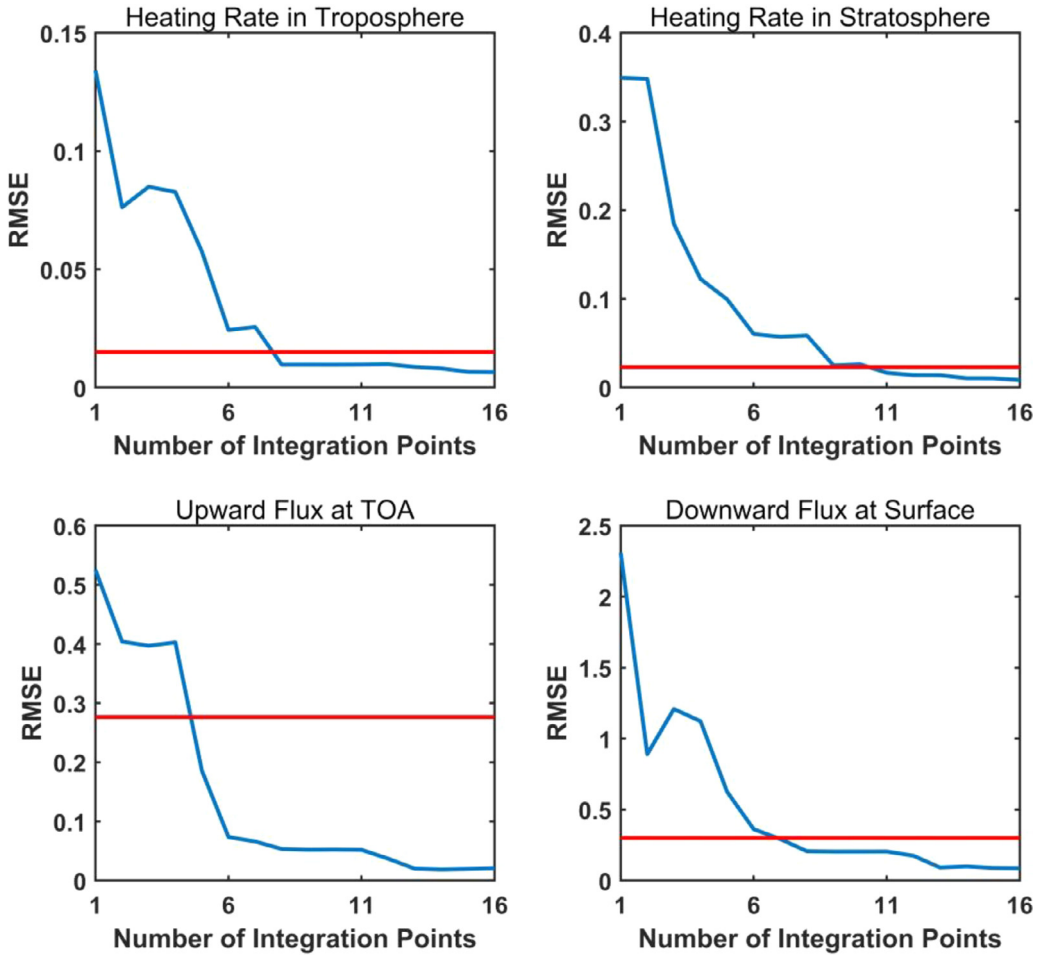

Fig. 8. a. RMSE of FPM versus the number of integration points in band 3 (500 - 630 cm^{-1}). The red line is the RMSE of RRTMG with 16 points. b. Maximum error of FPM versus the number of integration points in band 3 (500 - 630 cm^{-1}). The red lines are the error bounds of RRTMG with 16 points. The units of heating rate and flux are $Kday^{-1}$ and Wm^{-2}, respectively.

where

$$F^1_{err}(iatm) = \sqrt{\frac{\sum_{l=1}^{NL}\left(F^{\uparrow}(iatm,l,\Delta g_1,\Delta g_2,\ldots,\Delta g_M) - F^{\uparrow}_{LBL}(iatm,l)\right)^2}{\sum_{l=1}^{NL} F^{\uparrow}_{LBL}(iatm)^2}} + \sqrt{\frac{\sum_{l=1}^{NL}\left(F^{\downarrow}(iatm,l,\Delta g_1,\Delta g_2,\ldots,\Delta g_M) - F^{\downarrow}_{LBL}(iatm,l)\right)^2}{\sum_{l=1}^{NL} F^{\downarrow}_{LBL}(iatm,l)^2}}, \tag{14}$$

$$H^1_{err}(iatm) = \sqrt{\frac{\sum_{l=1}^{NL}\left(h(iatm,l,\Delta g_1,\Delta g_2,\ldots,\Delta g_M) - h_{LBL}(iatm,l)\right)^2}{\sum_{l=1}^{NL} h_{LBL}(iatm,l)^2}}, \tag{15}$$

and objective function 2 (OF2)

$$f^2_{obj}(\Delta g_1,\Delta g_2,\ldots,\Delta g_M) = \sqrt{\sum_{iatm=1}^{6}\left(F^2_{err}(iatm)^2 + H^2_{err}(iatm)^2\right)/6}, \tag{16}$$

where

$$F^2_{err}(iatm) = \sqrt{\sum_{l=1}^{NL}\left(F^{\uparrow}(iatm,l,\Delta g_1,\Delta g_2,\ldots,\Delta g_M) - F^{\uparrow}_{LBL}(iatm,l)\right)^2} + \sqrt{\sum_{l=1}^{NL}\left(F^{\downarrow}(iatm,l,\Delta g_1,\Delta g_2,\ldots,\Delta g_M) - F^{\downarrow}_{LBL}(iatm,l)\right)^2}, \tag{17}$$

$$H^2_{err}(iatm) = \sqrt{\sum_{l=1}^{NL}\left(h(iatm,l,\Delta g_1,\Delta g_2,\ldots,\Delta g_M) - h_{LBL}(iatm,l)\right)^2}, \tag{18}$$

and the variables in the objective functions are defined as follows: w_1,w_2,..., w_M are the weights of M integration points; $iatm$ and l are the ($iatm$)th atmospheric profile and lth level for atmospheric profiles; r is the ratio that set as 0.01; F^*_{err} and H^*_{err} are the errors of flux and heating rate, respectively; where $F^{\uparrow}_{LBL}$, $F^{\downarrow}_{LBL}$ and h_{LBL} are the LBL calculated value of upward flux, downward flux and heating rate, respectively; $F^{\uparrow}$ and $F^{\downarrow}$ and h are the CKD calculated value of upward flux, downward flux and heating rate, respectively. Fig. 5 shows the root mean squared errors (RMSEs) of heating rate, upward flux at TOA and downward flux at surface of two objective functions in band 5 (700-820 cm^{-1}) and band 9 (1180-1390 cm^{-1}). In band 5, the heating rate errors of OF1 are slightly less than OF2 in both troposphere and stratosphere. The upward flux errors of OF1 are larger than OF2 at all number cases, and the downward flux error of OF1 are larger than OF2 when the number of integration points is between 5 and 9. When the number of integration points is larger than 9, the downward flux errors of two functions are not much different. In band 9, the heating rate errors in tropo-

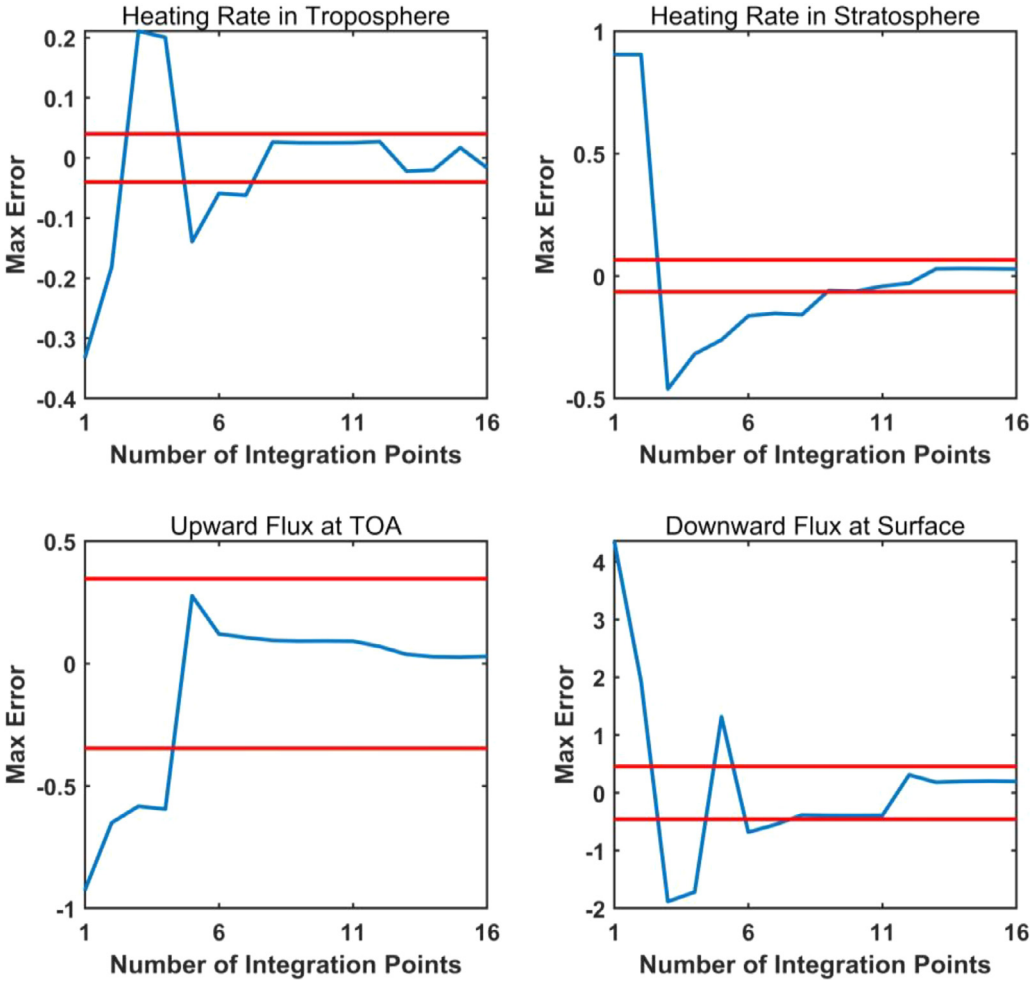

Fig. 8. Continued

sphere of two function do not have significant difference; the heating rate errors of OF1 in stratosphere are less than OF2 when the points are less than 9, and the RMSEs of two functions are almost the same while the number of integration points is larger than 9. For fluxes in two directions, the trend is similar with that in band 5. In conclusion, the results of OF2 is more accurate than that of OF1 when the number of integration points is large. Therefore, we used OF2 in our study.

3.2. Flux and heating rate

In our study, we set the vertical resolution of all standard profiles as 1 *km* and set TOA as 85 *km*, we used RRTMG's longwave spectral band division (10-2600 cm^{-1}), implemented gas species and the number of integration points in each band.

Table 3 illustrates the heating rate and radiative flux errors in all infrared spectral region calculated by ROM, FPM and RRTMG under six standard profiles. The accuracy of ROM is higher than FPM in downward flux, similar to FPM in heating rate, slightly lower in upward flux. Meanwhile, the accuracy of both ROM and FPM does not show a humble to RRTMG, and the errors of RRTMG are more than twice that of ROM and FPM. For the results of CO2 doubling concentration shown in Table 4, RRTMG still has the lowest accuracy. The accuracy of FPM is better than ROM in terms of maximum error of heating rate in stratosphere, RMSE and max error of upward flux at TOA. For the other results, ROM is better than FPM. In conclusion, ROM and FPM are more accurate than RRTMG.

Furthermore, we examined the accuracy of FPM and ROM in realistic atmospheric profiles. The atmospheric input profiles are from the ERA-Interim reanalysis data [23,24,25]. The data is monthly means of daily means in June, 2019, and the grid of the reanalysis data is in coarse resolution of 3° × 3°, and we average the data in the zonal direction. Fig. 6 shows the heating rate, upward flux and downward flux errors of FPM, ROM and RRTMG. For heating rate, the errors of RRTMG are small at the heights below 10 *hPa*, with a maximum value of 0.1 $Kday^{-1}$. In the high latitudes of the southern hemisphere at 5 *hPa*, there is a positive error center with a maximum value of 0.35 $Kday^{-1}$ approximately. Above 2 *hPa*, the error of RRTMG can reach above 1.5 $Kday^{-1}$. In contrast, the errors of FPM below 10 *hPa* are smaller than RRTMG, with a maximum error of about 0.09 $Kday^{-1}$. At the height 5 *hPa* of the low latitude area, FPM has a negative error center with the maximum value slightly higher than -0.25 $Kday^{-1}$. The errors of ROM are almost the same as FPM.

For upward flux, the errors of RRTMG are all negative values in the high latitudes of the southern hemisphere, and the maximum error is about -0.5 Wm^{-2}. At the height 100 *hPa* in the low latitudes of the southern hemisphere. There is a negative error center with the maximum is about -0.3 Wm^{-2}. The error in remaining areas are all positive values, and the error center is at an altitude of 40°N above 10 *hPa*. The maximum error is slightly higher than 1 Wm^{-2}. The errors of FPM are mostly negative values. The maximum error is at the height 20 *hPa* of 15°S, and the value is about -0.45 Wm^{-2}. The errors of ROM are almost all negative values. The

maximum error is at the height 2 *hPa* of 15°S, and the value is about -0.44 Wm^{-2}.

For downward flux, RRTMG has positive errors near 300 *hPa* in mid-high latitudes, and the errors in remaining areas are all negative values. The errors below 300 *hPa* are relatively large, with a maximum error of -2.22 Wm^{-2}. The errors of FPM above 200 *hPa* are small positive values, and the maximum error is only about 0.16 Wm^{-2}. The errors of FPM increase at the heights below 200 *hPa*. However, most errors do not exceed 0.9 Wm^{-2}. The largest error is at nearly 450 *hPa* in the high latitudes of the southern hemisphere, with a value about -1.2 Wm^{-2}. The error trend of ROM is similar with FPM. The maximum error of ROM above 200 *hPa* is about 0.38 Wm^{-2}, which is larger than that of FPM; while the maximum error of ROM below 200 *hPa* is about -0.56 Wm^{-2}, which is much lower than FPM.

For the condition of double CO2 concentration which the results are shown in Fig. 7, the error trends are similar with that in Fig. 6. The errors increase slightly for FPM, ROM and RRTMG. The maximum heating rate error of RRTMG increases to 0.5 $Kday^{-1}$, while the maximum errors of both FPM and ROM increase to -0.29 $Kday^{-1}$. The upward flux errors of RRTMG and FPM change to negative values. Therefore, the negative value area of RRTMG increases. The maximum negative error at 70°S increases to -0.53 Wm^{-2}, and the maximum positive error at 30°N decreases to 0.84 Wm^{-2}. The maximum error of FPM is slightly increased to -0.54 Wm^{-2}, and the maximum error of ROM decreases to -0.5 Wm^{-2}. The downward flux error of three methods do not change much.

Table 5
Number of integration points in FPM and RRTMG for each band.

Band	FPM	RRTMG
1	8	10
2	10	12
3	11	16
4	10	14
5	10	16
6	6	8
7	9	12
8	4	8
9	8	12
10	6	6
11	8	8
12	8	8
13	4	4
14	2	2
15	2	2
Total	106	138

3.3. Number of integration points

Since FPM and ROM can achieve high accuracy, we aimed to reduce the number of integration points. Fig. 8 show the RMSE (Fig. 8a) and the maximum error (Fig. 8b) of heating rate, upward flux at TOA and downward flux at surface of FPM in band 3 (500 - 630 cm^{-1}), and the comparison between FPM and RRTMG un-

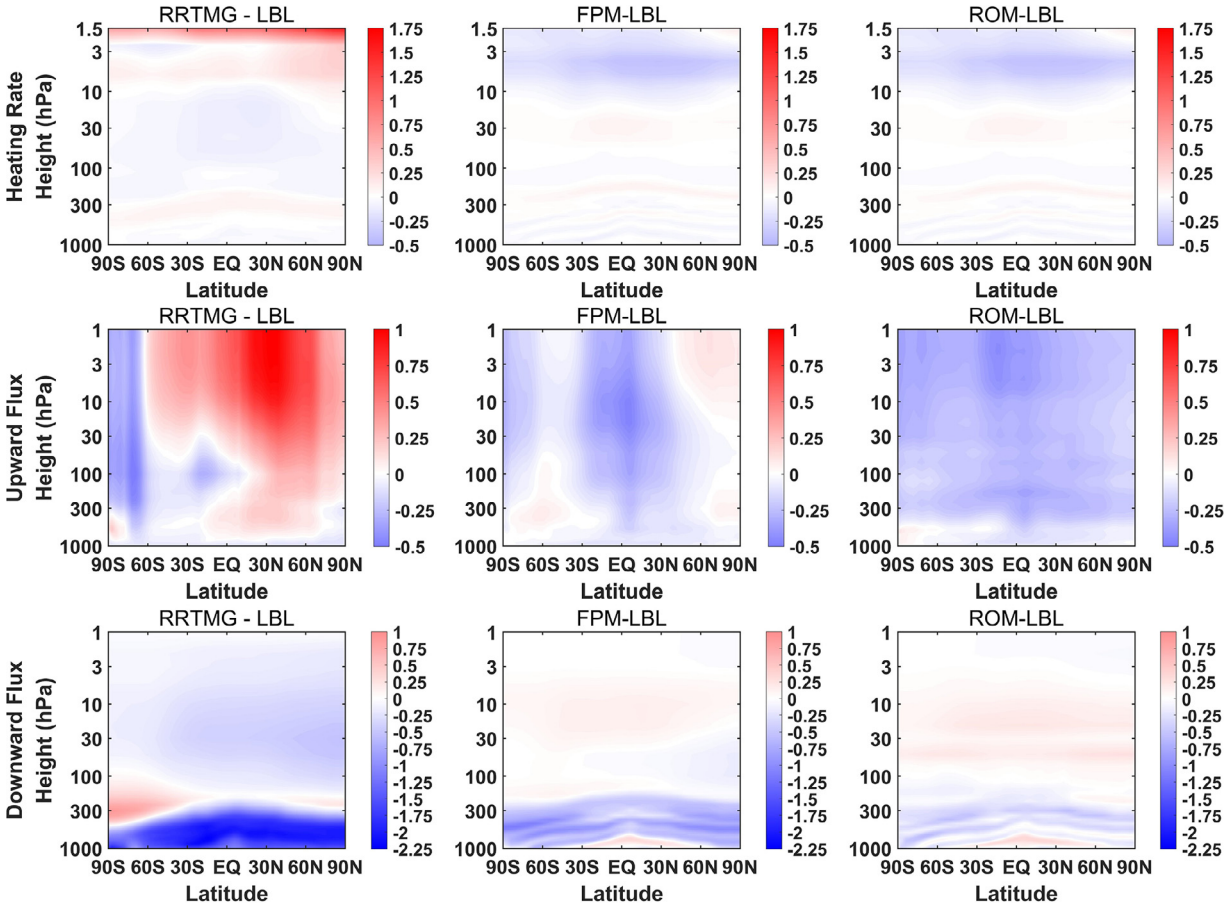

Fig. 9. Error contours for latitude-pressures calculated bi RRTMG with 138 points, FPM and ROM with 106 points. The units of heating rate and flux are $Kday^{-1}$ and Wm^{-2}, respectively.

der six standard profiles. The red lines in Fig. 8a are the RMSE of RRTMG with 16 integration points. FPM can get a smaller RMSE than RRTMG when the number of integration points are 8, 11, 5, 8 for heating rate in troposphere, heating rate in stratosphere, upward flux at TOA and downward flux at surface, respectively. The red lines in Fig. 8b are the error bounds of RRTMG with 16 integration points. The max errors of FPM are smaller than RRTMG when the number of integration points are 8, 9, 5, 8 for heating rate in troposphere, heating rate in stratosphere, upward flux at TOA and downward flux at surface, respectively. Summarize two comparisons, we can get a conclusion that FPM can achieve higher accuracy than RRTMG when the number of integration points is only 11, which is almost 1/3 less than RRTMG.

Table 5 shows the number of integration points of FPM and RRTMG for all bands when the accuracy of the two is similar. The total number of FPM is 32 less than that of RRTMG, which is over 1/5 less than RRTMG. Furthermore, we examined the accuracy of FPM and ROM with 106 points in realistic atmospheric profiles, the results are shown in Fig. 9. Compared with the results of FPM with 138 points, the accuracy of FPM with 106 points decreases after reducing the number of integration points. In the upper atmosphere at 5 *hPa*, the maximum heating rate errors of FPM and ROM are both 0.4 $Kday^{-1}$, which are only 0.045 $Kday^{-1}$ larger than that of RRTMG. For the upward and downward fluxes, the accuracy of FPM and ROM does not change much. For upward flux, the maximum error of FPM slightly increases to -0.46 Wm^{-2}, and the maximum error of ROM decreases to -0.43 Wm^{-2}. For downward flux, the maximum error of FPM at 20 *hPa* increases to 0.36 Wm^{-2}, and the maximum error below 200 *hPa* is slightly decreases to -1.14 Wm^{-2}; the maximum error of ROM at 20 *hPa* slightly decreases to 0.37 Wm^{-2}, and the maximum error below 200 *hPa* slightly increases to -0.59 Wm^{-2}. In conclusion, the accuracy of FPM and ROM is still higher than that of RRTMG.

4. Conclusions and Discussion

Two automatic methods for gas absorption calculation based on correlated k-distribution are proposed, namely so-called finding point method and re-optimized method. Compared with the DM, we changed the calculation process of the optimization algorithm and improved the accuracy of the method. Both ROM and FPM are more accurate than RRTMG.

For both standard profiles and realistic profiles, ROM is more accurate than FPM in downward flux, but less accurate in upward flux accuracy. This is because in the secondary optimization process of ROM, in order to minimize the objective function, SQP reduces the large value in the error, but sometimes also makes the small value larger. The error distribution becomes more uniform. Therefore, under the realistic atmospheric profiles, the downward flux error of FPM can reach 1.2 Wm^{-2}. In contrast, the maximum downward flux error of ROM is only 0.56 Wm^{-2}, which is less than half that of FPM.

The number of integration points of FPM and ROM is reduced. The total number of points is 106 for both FPM and ROM, which is 32 less than that of RRTMG. The accuracy of the methods under the realistic profile condition is examined. The accuracy of FPM slightly decreases after the number of integration points reduced. In the upper atmosphere at 5 *hPa*, the maximum heating rate errors of FPM and ROM are slightly larger than that of RRTMG. For the upward and downward fluxes, the accuracy of FPM and ROM do not have significant changes. In conclusion, the accuracy of FPM and ROM is still higher than that of RRTMG.

Here the HITRAN2016 spectral database [26] and MT_CKD 3.1 are used in our calculation, which may be the reason for the low accuracy of RRTMG. According to the comparison between different versions of HITRAN databases, the downward flux differences between HITRAN2008 and HITRAN2016 are all negative values for standard profiles, and the upward flux differences are all positive values [27]. Furthermore, that trend of positive and negative values is similar with the error results of RRTMG in our calculation. Besides, we used six standard atmospheric profiles under clear sky in the objective function. Therefore, we might be able to make FPM and ROM more accurate by increasing the number of standard profiles and adding scattering atmospheres. Because the results optimized based on six standards, and might not be the optimal solution under other atmospheric profiles. For example, in our study, the accuracy of the results under the realistic atmospheric profiles is lower than that of the standard profile.

Funding

This work was supported by the Jiangsu Province Distinguished Professor Project (Grant No. R2018T20); and the Startup Foundation for Introducing Talent of NUIST (Grant No. 2018R037).

Declaration of Competing Interest

The authors declare that they have no known competing financial interests or personal relationships that could have appeared to influence the work reported in this paper.

CRediT authorship contribution statement

Mingwei Zhu: Conceptualization, Methodology, Software, Writing - original draft, Writing - review & editing. **Shuanggen Jin:** Supervision, Writing - review & editing. **Ju Tao:** Data curation. **Xinyue Wu:** Data curation.

Acknowledgment

Authors acknowledged Atmospheric and Environmental Research, Inc. (AER, inc.) for providing open source codes of Line-By-Line Radiative Transfer Model, and Rapid Radiative Transfer Model for General Circulation Models (RRTMG).

References

[1] Clough SA, Iacono MJ, Moncet J. L Line-by-line calculation of atmospheric fluxes and cooling rates: Application to water vapor. J Geophys Res 1992;97:15761–85.
[2] Clough SA, Iacono MJ. Line-by-line calculations of atmospheric fluxes and cooling rates. Part II: Application to carbon dioxide, ozone, methane, nitrous oxide, and the halocarbons. J Geophys Res 1995;100:16519–35.
[3] Edwards DP. GENLN2: A general line-by-line atmospheric transmittance and radiance model, Version 3.0 description and users guide, NCAR/TN-3674-STR. National Center for Atmospheric Research; 1992.
[4] Zhang H, Shi G, Nakajima T, Suzuki T. The effects of the choice of the k-interval number on radiative calculations. J Quant Spectrosc Radiat Transf 2006;98:31–43.
[5] Zhang F, Zhu M, et al. Alternate Mapping Correlated k-Distribution Method for Infrared Radiative Transfer Forward Simulation. Remote Sens 2019;11:994.
[6] Arking A, Grossman K. The influence of line shape and band structure on temperatures in planetary atmospheres. J Atmos Sci 1972;29:937–49.
[7] Gerstell MF. Obtaining the cumulative k-distribution of a gas mixture from those of its components. J Quant Spectrosc Radiat Transf 1993;49(1):15–38.
[8] Goody R, West R, et al. The correlated k method for radiation calculations in nonhomogenous atmospheres. J Quant Spectrosc Radiat Transf 1989;42:539–50.
[9] Li J, Barker HW. A radiation algorithm with correlated k distribution. Part 1: Local thermal equilibrium. J Atmos Sci 2005;62:286–309.
[10] Shi G, Xu N, Wang B, et al. An improved treatment of overlapping absorption bands based on the correlated k distribution model for thermal infrared radiative transfer calculations. J Quant Spectrosc Radiat Transf 2009;110:435–51.
[11] Zhang H, Nakajima T, Shi G, et al. An optimal approach to overlapping bands with correlated k-distribution method and its application to radiative calculations. J Geophys Res 2003;108:4641–53.
[12] Fu Q, Liou KN. On the correlated k distribution method for radiative transfer in nonhomogeneous atmospheres. J Atmos Sci 1992;49:2139–56.
[13] Lacis AA, Oinas V. A description of the correlated k-distribution method modeling non-grey gaseous absorption, thermal emission, and multiple scattering in vertical inhomogeneous atmosphere. J Geophys Res 1991;96:9027–63.

[14] Shi G. Effect of atmospheric overlapping bands and their treatment on the calculation of thermal radiation. Adv Atmos Sci 1984;1:246–55.
[15] Mlawer EJ, Taubman SJ, Brown PD, et al. Radiative transfer for inhomogeneous atmosphere: RRTM, a validated correlated-k model f or the longwave. J Geophys Res 1997;102(D14):16663–82.
[16] Morcrette JJ. Radiation and cloud radiative properties in the European Center for Medium Range Weather Forecasts Forecasting System. J Geophys Res 1991;96:9121–32.
[17] Iacono MJ, MlawerEJ Clough SA, Morcrette JJ. Impact of an improved longwave radiation model, RRTM, on the energy budget and thermodynamic properties of the NCAR community climate model, CCM3. J Geophys Res 2000;105:14873–90.
[18] Wang WC, Ryan PB. Overlapping effect of atmospheric H2O, CO2 and O3 on the CO2 radiative effect. Tellus, Ser. B 1983;35:81–91.
[19] Nakajima T, Tsukamoto M, Tsushima Y, Numaguti A, Kimura T. Modeling of the radiative process in an atmospheric general circulation model. Appl Opt 2000;39(27):4869–78.
[20] Sekiguchi M, Nakajima T. A k-distribution-based radiation code and its computational optimization for an atmospheric general circulation model. J Quant Spectrosc Radiat Transf 2008;109:2779–93.
[21] Ibaraki T, Fukushima M. FORTRAN77 optimization programming. Tokyo: Iwanami-shoten; 1991. p. 480.
[22] McClatchey RA, Fenn RW, Selby JE, et al. Optical properties of the atmosphere. Optical Physics Laboratory, Air Force Cambridge Research Laboratories 1972:1–108.
[23] Dee DP, Ippala SM. The ERA-Interim reanalysis: Configuration and performance of the data assimilation system. Quart J R Meteorol Soc 2011;137:553–97.
[24] Simmons AJ, Poli P, Dee DP, et al. Estimating low-frequency variability and trends in atmospheric temperature using ERA-Interim. Quart J R Meteorol Soc 2014;140:329–53.
[25] Simmons AJ, Willett KM, Jones PD, et al. Low-frequency variations in surface atmospheric humidity, temperature and precipitation: Inferences from reanalyses and monthly gridded observational datasets. J Geophys Res 2010;115:D01110.
[26] Gordon IE, Rothman LS, et al. The HITRAN2016 molecular spectroscopic database. J Quant Spectrosc Radiat Transf 2017;203:3–69.
[27] Zhu M, Zhang F, et al. The impact of various HITRAN molecular spectroscopic databases on infrared radiative transfer simulation. J Quant Spectrosc Radiat Transf 2019;234:55–63.